Received: 5 October 2022 | Accepted: 1 November 2022

DOI: 10.1002/pamm.202200085

Data-based prediction of the viscoelastic behavior of short fiber reinforced composites

Julian Marr[1,*], **Lukas Zartmann**[1], **Doris Reinel-Bitzer**[1], **Heiko Andrä**[2], and **Ralf Müller**[3,**]

[1] ZF Friedrichshafen AG, Research and Development, Friedrichshafen, Germany
[2] Fraunhofer Institute for Industrial Mathematics ITWM, Department of Flow and Material Simulation, Kaiserslautern, Germany
[3] Technical University of Darmstadt, Institute for Mechanics, Darmstadt, Germany

The viscoelastic behavior of short fiber reinforced polymers (SFRPs) partly depends on different microstructural parameters such as the local fiber orientation distribution. To account for this by simulation on component level, two-scale methods couple simulations on the micro- and macroscale, which involve considerable computational costs. To circumvent this problem, the generation of a viscoelastic surrogate model is presented here. For that purpose, an adaptive sampling technique is investigated and data are obtained by creep simulations of representative volume elements (RVEs) using a fast Fourier transform (FFT) based homogenization method. Numerical tests confirm the high accuracy of the surrogate model. The possibility of using that model for efficient material optimization is shown.

1 Introduction

SFRPs are extensively used for engineering applications [11] because they combine attractive features like low density and ease of fabrication with high stiffness and strength. To study the long-term and rate-dependent behavior of SFRP parts, the use of simulation is useful since very time-consuming tests can be partially replaced. For that purpose, the knowledge of the effective viscoelastic behavior is of fundamental importance. Production by injection molding usually leads to locally different fiber orientations in the component. These orientations on the microscale have a great influence on the effective material behavior. By performing multiscale simulations, many similar problems accounting for that local microstructure information have to be solved [3]. Especially for complex structures, that approach is associated with significant computational effort. To overcome this, data-driven approaches [14] are gaining popularity in the past few years, where machine learning (ML) models are used to reproduce micromechanical simulations. In this paper, the idea of surrogate modeling is introduced to construct an effective viscoelastic model for different (arbitrary) microstructural parameters. As microstructural parameters, the local fiber orientation distribution, the fiber volume fraction and the linear elastic properties of the fiber material are investigated. A generalized Maxwell model [2] is considered as viscoelastic material model for the polymer matrix and the associated material parameters are identified by an experimentally determined master curve. An adaptive sampling scheme based on a bias-variance decomposition is used to efficiently explore the space of microstructural parameters. The samples are evaluated by performing numerical homogenization [1, 10, 12, 13] on RVEs [5]. Beside using the model for an efficient two-scale simulation, it will be shown that such a model can be applied to solve an inverse problem. In order to design materials with desired properties, a formulation as parameter optimization problem accounting for different microstructural descriptors is presented. Using the surrogate model for the solution of that optimization problem with global optimization methods enables an efficient determination of optimized microstructures.

2 Microscopic structure and material input parameters

2.1 Parametrization of the microstructure

For the representation of the local fiber orientation state, the second-order symmetric Advani-Tucker tensor [9] is employed. By making use of a principal component analysis, that tensor can be expressed in terms of an orthogonal rotation matrix defined by three Euler angles θ, γ, β and a diagonal matrix with eigenvalues λ_1, λ_2 and λ_3 with $\lambda_1 + \lambda_2 + \lambda_3 = 1$. Different fiber orientation states can be visualized within the constrained fiber orientation triangle spanned by λ_1 and λ_2. In [3], a special coloring scheme is introduced in order to visualize theses different orientation states. All investigated material parameters are listed in Table 1 and are chosen such that many SFRPs relevant in industrial applications can be considered. The Sequential Addition and Migration (SAM) method [5] is used for the virtual generation of RVEs of short fiber reinforced polymers. The fiber length is specified to be constant with 200 µm and an aspect ratio (=fiber length/fiber diameter) of 20 is chosen, because these are typical values for industrially used SFRPs. For arbitrary fiber orientation states, the tangential stiffness tensor can be calculated in a post-processing step by specification of the angles θ, γ, β.

* e-mail julian.marr@zf.com
** Corresponding author: e-mail ralf.mueller@mechanik.tu-darmstadt.de

Table 1: Microstructure descriptor with lower- and upper bounds.

Index i	Microstructure Descriptor d_i	Lower bound $d_{i,low}$	Upper bound $d_{i,up}$
1	Fiber volume fraction [%]	5	20
2	Fiber orientation state λ_1 [-]	$0.3\overline{3}$	1
3	Fiber orientation state λ_2 [-]	$0.5(1-\lambda_1)$	$\min(\lambda_1, 1-\lambda_1)$
4	Young's modulus fibers [GPa]	25	180
5	Poisson's ratio fibers [-]	0.2	0.4
6	θ [rad]	0	π
7	γ [rad]	0	π
8	β [rad]	0	π

2.2 Viscoelastic material model and parameter identification of the matrix material

In order to describe the viscoelastic behavior of the polymer matrix, a generalized Maxwell model [2] is used. The stresses $\boldsymbol{\sigma}$ and strains $\boldsymbol{\epsilon}$ are linked in linear viscoelasticity via a convolution integral taking into account arbitrary strain histories by the superposition principle:

$$\boldsymbol{\sigma}(t) = \int_0^t \boldsymbol{\Gamma}(t-s) : \frac{\partial \boldsymbol{\epsilon}(s)}{\partial s} ds. \tag{1}$$

In (1), $\boldsymbol{\Gamma}$ describes a symmetric fourth-order relaxation tensor. It will be assumed that for the generalized Maxwell model (sketched as rheological model in Fig. 1), the relaxation tensor can be expressed as

$$\boldsymbol{\Gamma}(t) = \psi(t)\boldsymbol{C}^r \tag{2}$$

with the normalized relaxation function

$$\psi(t) = 1 + \sum_{k=1}^{N} \gamma_k \exp\left(\frac{t}{\tau_k}\right), \tag{3}$$

and the normalized relaxation coefficients $\gamma_k = \frac{E_k}{E_0}$. For $t \to \infty$, $\boldsymbol{\Gamma}(t)$ tends to the relaxed stiffness tensor $\boldsymbol{C}^r$ and leads to a purely linear elastic (relaxed) material described by a single spring element. In this paper, PA66 (Zytel 101) is investigated as matrix material and the behavior of the polymer is assumed to be isotropic with Poisson's ratio $\nu = 0.38$. For the material model (1), the material parameters E_k and τ_k (respectively $\eta_k := E_k \cdot \tau_k, k = 1, ..., N$) have to be determined. In [8], corresponding measurements including a master curve for this polymer material are given. 10 Maxwell elements ($N = 10$, one for every time decade) are used to approximate the master curve in the time range from $t \in [0, 10^{10}]$s and the relaxation constants τ_k are specified to be constant (see Table 2). The stiffness parameters E_k and E_0 are determined by solving a least squares optimization problem considering the differences in the strain values from the master curve and the numerical model with the sequential quadratic programming (SQP) method. The identified viscoelastic material parameters are summarized in Table 2. The fibers are modeled as linear elastic (isotropic) and can be described by the specification of a Young's modulus and a Poisson's ratio (see Table 1).

Table 2: Material parameters of the generalized Maxwell model ($N = 10$).

Maxwell Element k	E_k [MPa]	τ_k [s]	γ_k [-]
0	498.45	-	-
1	47.40	1e+01	0.095
2	15.00	1e+02	0.030
3	187.61	1e+03	0.376
4	197.39	1e+04	0.396
5	200.04	1e+05	0.401
6	200.30	1e+06	0.402
7	145.39	1e+07	0.292
8	99.91	1e+08	0.200
9	51.24	1e+09	0.103
10	20.35	1e+10	0.041

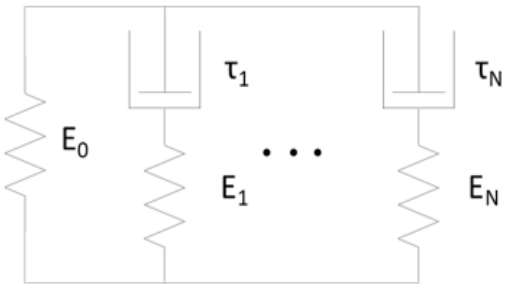

Fig. 1: Principal sketch of the generalized Maxwell model.

3 Construction of a viscoelastic surrogate model

3.1 Initial and adaptive sampling strategy

In Fig. 2, a flowchart of the data-based material analysis and design framework is shown. In a first step, based on a Design of Experiment (DoE) scheme, predefined samples in the material parameter space are selected. For that purpose, the space-filling Latin Hypercube sampling (LHS) [7] scheme is chosen, and 12 samples are selected for the construction of an initial surrogate. For each of these samples, an RVE is created and six boundary value problems (3 tensile and 3 shear loads in perpendicular coordinate directions) are solved by FFT-based homogenization [1, 12, 13] using 8 time increments per decade equally spread over a logarithmic time scale. As quantity of interest, the orthotropic components of the creep compliance tensor are investigated because the other parameters are quite small compared to these components. These orthotropic material parameters are described by three Young's moduli, three shear moduli and three Poisson's ratios and can be identified in the creep compliance tensor (in Voigt notation) as follows:

$$\boldsymbol{\Upsilon}(t) = \begin{bmatrix} \frac{1}{E_1(t)} & -\frac{\nu_{21}(t)}{E_2(t)} & -\frac{\nu_{31}(t)}{E_3(t)} & 0 & 0 & 0 \\ -\frac{\nu_{12}(t)}{E_1(t)} & \frac{1}{E_2(t)} & -\frac{\nu_{32}(t)}{E_3(t)} & 0 & 0 & 0 \\ -\frac{\nu_{13}(t)}{E_1(t)} & -\frac{\nu_{23}(t)}{E_2(t)} & \frac{1}{E_3(t)} & 0 & 0 & 0 \\ 0 & 0 & 0 & \frac{1}{G_{23}(t)} & 0 & 0 \\ 0 & 0 & 0 & 0 & \frac{1}{G_{13}(t)} & 0 \\ 0 & 0 & 0 & 0 & 0 & \frac{1}{G_{12}(t)} \end{bmatrix}. \tag{4}$$

For each of these orthotropic parameters, a Kriging interpolation model [4] is generated. The time-dependence is modeled on the logarithmic time scale. This means that in the considered time domain $t \in [0.133, 10^{10}]$s, 11 time-steps in the logarithmic time domain (one for the first time-increment and one for every decade $(10^1, 10^2, ..., 10^{10})$s) are used for each microstructural sample. In order to refine the initial Kriging model, the expected improvement for global fit (EIGF) criterion [6] is investigated as learning function. That learning function can be expressed by a bias-variance decomposition as

$$\mathrm{EIGF}(d) = (\hat{f}(d) - f(d_k))^2 + \sigma^2(d). \tag{5}$$

where the first term is the bias term with $\hat{f}(d)$ being the Kriging prediction at d and $f(d_k)$ being the true response of the nearest (measured in the normalized Euclidean distance) sampling point d_k related to d. The variance term $\sigma^2(d)$ results

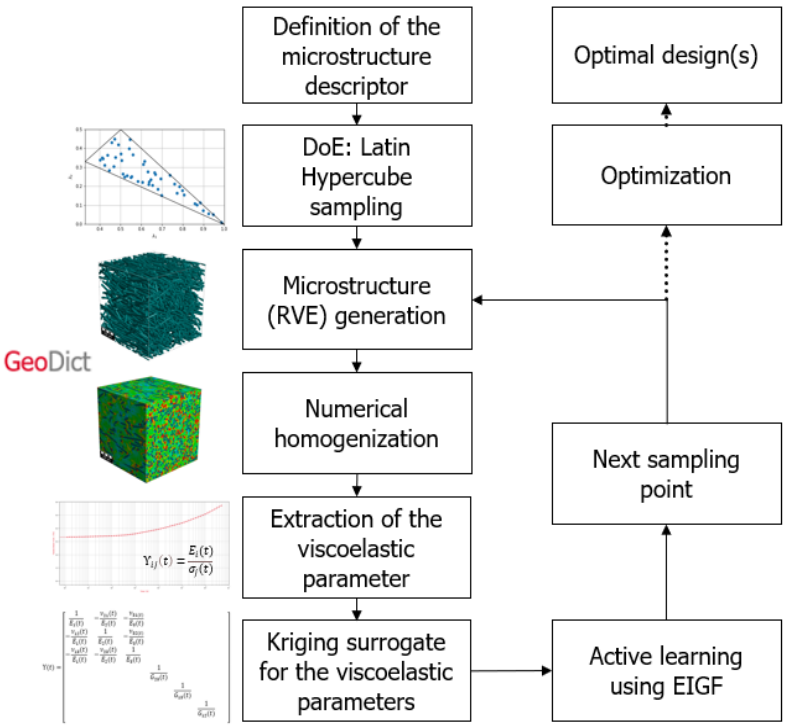

Fig. 2: Data-based viscoelastic material analysis and design framework

directly from the Kriging interpolation. For the determination of the next sampling point, the so-called infill sampling criteria, the maximum of the EIGF-function is considered:

$$d_{next} = \underset{d}{\text{argmax}}\ \text{EIGF}(d) \qquad \text{s. t.} \quad d_{i,low} \leq d \leq d_{i,up}. \tag{6}$$

Based on (6), 24 samples are selected to refine the surrogate, so in total $n_{samp} = (12 + 24) \cdot 11 = 396$ samples are used for the building of the surrogate models. The created database is described as n_{samp} sets of six inputs $d \in \mathbb{R}^6$ (since the orthotropic constants are time-dependent, the time can be assumed as additional parameter) and the nine orthotropic parameters $y \in \mathbb{R}^9$ ($y \rightarrow E_1, E_2, E_3, G_{23}, G_{13}, G_{12}, \nu_{23}, \nu_{13}, \nu_{12}$) as outputs as

$$\{(d^{(1)}, y^{(1)}), (d^{(2)}, y^{(2)}), ..., (d^{(n_{samp})}, y^{(n_{samp})})\}. \tag{7}$$

After each adaptive sampling step, a new Kriging model is generated. The samples (initial in blue, adaptive in red) in the geometrical microstructure (top, a), b)) and in the fiber material property descriptor space (bottom, c), d)) are shown in Fig. 3 for E_1 (left, a), c)) and for G_{12} (right, b), d)). One can observe a good distribution of the samples within the entire microstructure descriptor spaces. Many of the adaptive samples are selected along the edges of the fiber orientation triangle. By adding more samples, the inner area of the triangle gets explored. In Fig. 4, the RVEs for two samples (unidirectional a) and isotropic fiber orientation b)) are illustrated. In Fig. 5, the associated stress fields (von Mises) within a cross-sectional area (half RVE length) by specification of a macroscopic tensile load of 1 MPa in fiber direction a) and a macroscopic shear load of 1 MPa b) are shown for t=10,000s. As expected, the highest stresses can be found in the fiber material, leading to a highly anisotropic macroscopic material behavior.

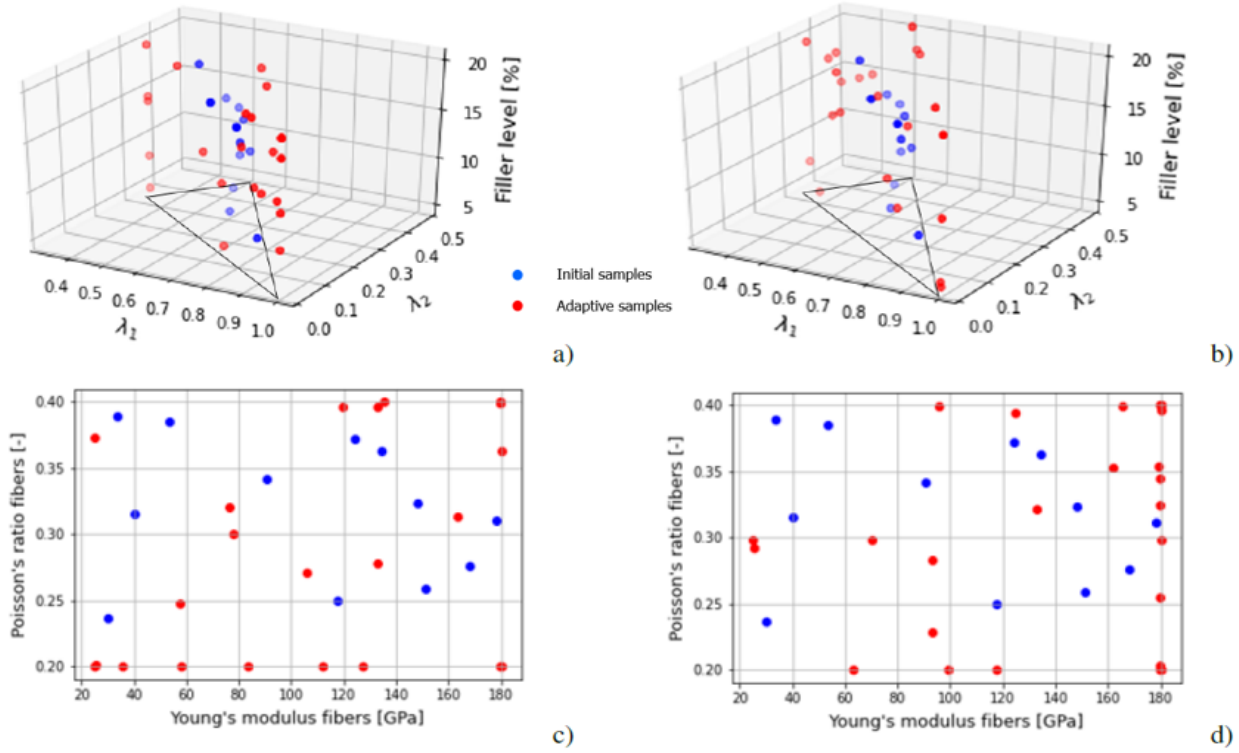

Fig. 3: Sample distribution in the geometrical microstructure (top, a), b)), and fiber material property descriptor space (bottom, c), d)) for E_1 (left, a), c)) and G_{12} (right, b), d))

3.2 Surrogate model validation

In order to assess the quality of the surrogate models, an error analysis using 20 % of all samples (randomly selected) as validation data is performed. For that purpose, in Fig. 6, the surrogate results are plotted against the predictions of the numerical model for the component E_1 (left) and G_{12} (right). It can be observed that the Kriging interpolation shows high prediction accuracy. For both models, as quantitative error criteria, the coefficient of determination (CoD) is computed. A CoD-value of 1.0 confirms the high fidelity of the surrogate models. If the quality of the model would not be sufficient, more infill samples could be computed to improve the prediction quality of the model.

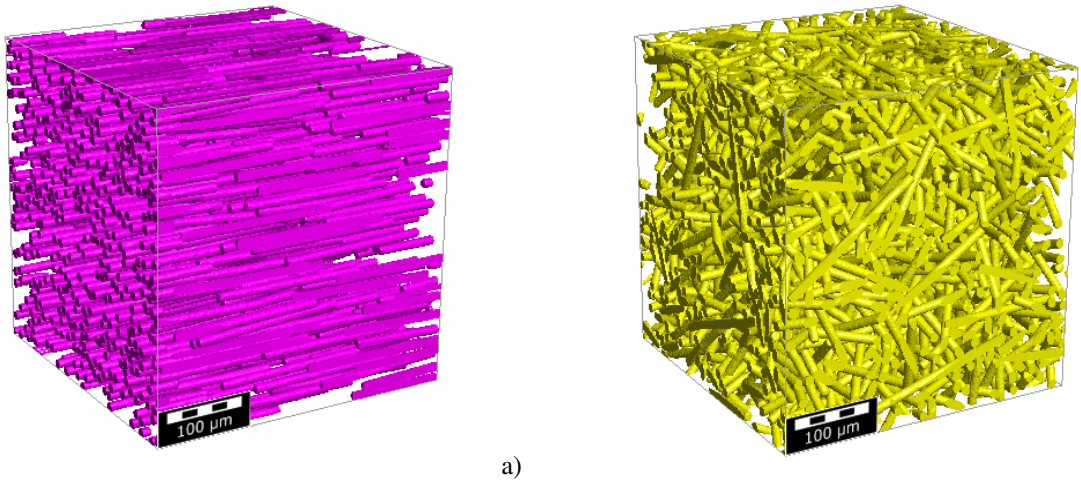

Fig. 4: RVE of samples: a) Unidirectional ($d_2 = 1, d_3 = 0$) fiber orientation with fiber volume fraction $d_1 = 18.08$ %, b) isotropic fiber orientation ($d_2 = d_3 = 0.3\overline{3}$) with $d_1 = 19.87$ %.

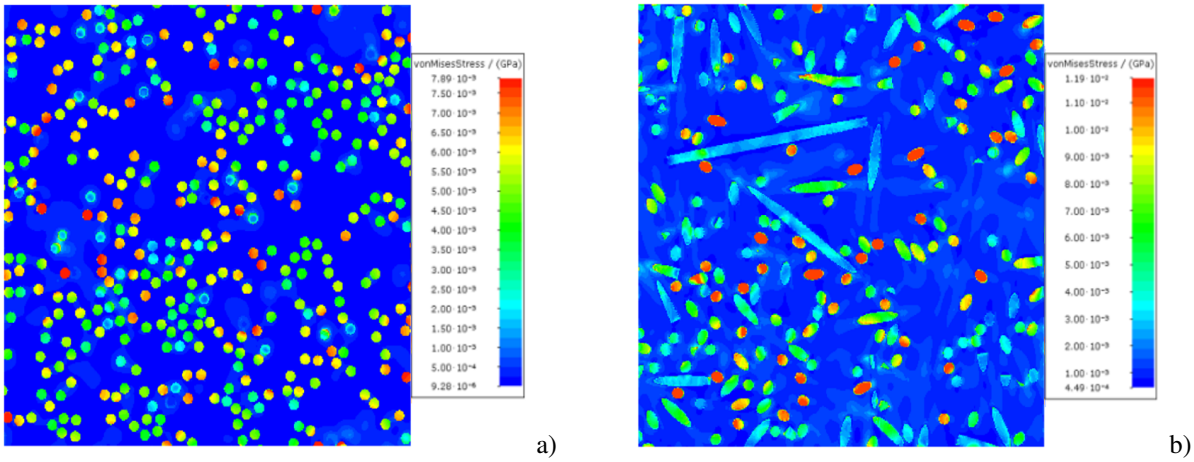

Fig. 5: Von Mises stress within a cross-sectional area (half RVE length) of the associated RVEs by specification of: a) A macroscopic tensile load of 1 MPa in fiber direction with the fiber material propertys $d_4 = 180$ GPa and $d_5 = 0.2$, b) a macroscopic shear load of 1 MPa with $d_4 = 63.10$ GPa and $d_5 = 0.2$ after t=10,000s.

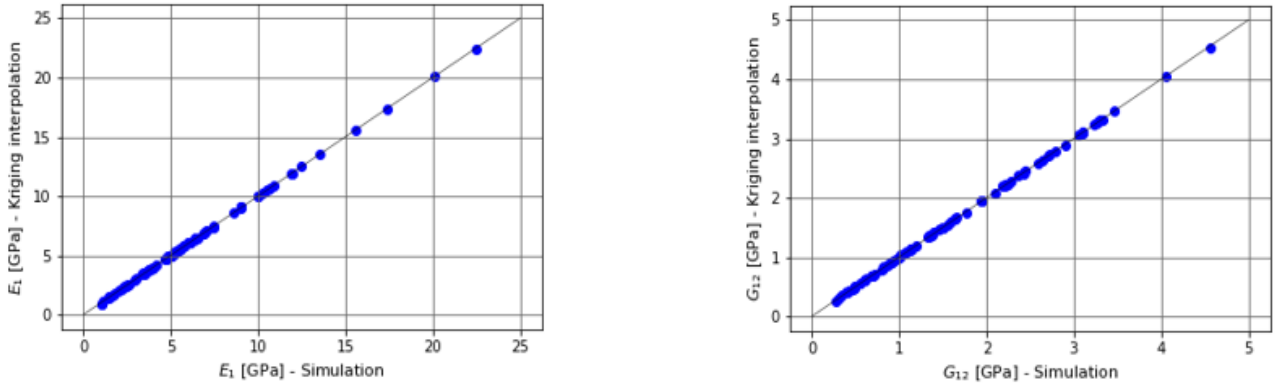

Fig. 6: Comparison of the Kriging predictions with the micromechanical results for E_1 (left) and G_{12} (right)

3.3 Parametric material optimization

In technical applications, it often occurs that desired material properties are specified to fulfill desired product requirements. In order to find an optimal microstructural design with target viscoelastic behavior, the following parametric minimization problem for the design variables d is introduced:

$$\begin{aligned} J(d) &= \left\| \frac{\boldsymbol{\Upsilon}(d) - \boldsymbol{\Upsilon}^*}{\boldsymbol{\Upsilon}^*} \right\|_2 \rightarrow \min \\ \text{s. t.} \qquad & d_{i,low} \leq d \leq d_{i,up}. \end{aligned} \tag{8}$$

In (8), $\boldsymbol{\Upsilon} = \boldsymbol{\Upsilon}(d)$ describes the creep compliance tensor in dependence of the design variables d, and $\boldsymbol{\Upsilon}^*$ is the target creep compliance tensor. A further analysis of optimization problem (8) shows that the use of gradient-based optimization methods possesses difficulties. The stochastic nature of the RVEs leads to mutual fluctuations in the considered strain and stress fields, which, in turn, leads to noise in the objective function. Even if the optimization is performed on the surrogate model, the influence of such noise or deviations of the generated geometrical microstructure from the specification exhibits non-convexity of the objective function leading to get stuck in a local optimum when gradient-based optimization techniques are used. Furthermore, it is likely that non-convexity is encountered due to the diversity of design parameters. Due to these reasons, a global optimization method such as differential evolution seems appropriate for the solution of (8). Using such global methods on the direct numerical model leads to tremendous numerical effort, because in every iteration an RVE has to be generated and six boundary value problems have to be solved. If the optimization is performed on the surrogate model, the function evaluations in every iteration can be performed very fast and the computational effort is drastically reduced. By locally influencing the microstructure during the manufacturing process, the results of the material optimization can be taken into account to achieve a required macroscopic viscoelastic behavior.

4 Conclusion

In this paper, a surrogate model of the effective viscoelastic behavior of short fiber reinforced composites was presented. For an efficient exploration of the constraint design space, an infill sampling criterion was used. Numerical tests show a high predictive quality of the surrogate model. Therefore, the surrogate model can be used for efficient multiscale optimization. The proposed methodology has a generalization ability and can be extended to the optimal material design for a wide range of composites and various other effective material properties.

Acknowledgements Open access funding enabled and organized by Projekt DEAL.

References

[1] H. Moulinec and P. Suquet, Comput. Methods Appl. Mech. Eng. **157**, 69–94 (1998).
[2] M. Kaliske and H. Rothert, Comput. Mech. **19**, 228–239 (1997).
[3] J. Köbler, M. Schneider, F. Ospald, H. Andrä and R. Müller, Comput. Mech. **61**, 729–750 (2018).
[4] T. W. Simpson, D. K. Lin, and W. Chen, Int. J. Reliab. **2**, 209–240 (2001).
[5] M. Schneider, Comput. Mech. **59**, 247–263 (2017).
[6] C. Q. Lam, Ph.D. thesis, The Ohio State University, Columbus.
[7] R. Jin, W. Chen, and A. Sudjianto, J. Stat. Plan. Inference **134**, 268-287 (2005).
[8] J. L. Yang, Z. Zhang, A. K. Schlarb, and K. Friedrich, Polymer **47**, 6745-6758 (2006).
[9] S. G. Advani and C. L. Tucker, Polymer **31**, 751–784 (1987).
[10] J. Becker, F. Biebl, E. Glatt, L. Cheng, A. Grießer, M. Groß, S. Linden, D. Mosbach, C. Wagner, A. Weber, and R. Westerteiger, GeoDict (Release 2022) [Simulation software], Math2Market GmbH, doi.org/10.30423/release.geodict2022.
[11] J. Kuruvilla, O. Kristiina, G. Gejo, W. Runcy, and A. Saritha (eds.), Fiber Reinforced Composites (Woodhead Publishing, Sawston, 2021), 785-819.
[12] M. Kabel, A. Fink, and M. Schneider, Comput. Methods Appl. Mech. Eng. **322**, 396-418 (2017).
[13] M. Kabel, S. Fliegener, and M. Schneider, Comput. Mech. **57**, 193-210 (2016).
[14] M. A. Bessa et al., Comput. Methods Appl. Mech. Eng. **320**, 633-667 (2017).

